



Hydrophobicity-enhanced magnetic solid sulfonic acid: A simple approach to improve the mass transfer of reaction partners on the surface of the heterogeneous catalyst in water-generating reactions



Akbar Mobaraki ^{a,1}, Barahman Movassagh ^{a,*}, Babak Karimi ^{b,2}

^a Department of Chemistry, K.N. Toosi University of Technology, P.O. Box 16315-1618, Tehran, Iran

^b Department of Chemistry, Institute for Advanced Studies in Basic Sciences (IASBS), Gava Zang, Zanjan 45137-66731, Iran

ARTICLE INFO

Article history:

Received 24 September 2013

Received in revised form

11 December 2013

Accepted 12 December 2013

Available online 22 December 2013

Keywords:

Heterogeneous catalyst

Hydrophobicity

Water-tolerance

Mass transfer

Solid acid

Core-shell magnetic nanoparticles

Biginelli reaction

ABSTRACT

Two novel and environmentally benign organosulfonic acid-functionalized silica-coated magnetic nanoparticle catalysts **1** ($\text{Fe}_3\text{O}_4@\text{SiO}_2@\text{Et-PhSO}_3\text{H}$) and **2** ($\text{Fe}_3\text{O}_4@\text{SiO}_2@\text{Me&Et-PhSO}_3\text{H}$) were prepared and their surface hydrophobicity was assessed by esterification reaction of fatty alcohols. Also, their water-tolerance in two water-generating reactions was investigated, namely: synthesis of bis(indolyl)methane and the Biginelli reaction of benzaldehyde, methyl acetoacetate, and urea under solvent-free conditions. In these reactions, the catalyst **2** that was more hydrophobic and water-resistant showed higher catalytic activity and was characterized extensively by various techniques. This catalyst was successfully used in the Biginelli reaction of a series of aldehydes, β -keto esters, and urea/thiourea for the synthesis of a diverse range of pharmacologically active 3,4-dihydropyrimidin-2-one/thione (DHPM) derivatives. The catalyst **2** was easily separated by an external magnet and the recovered catalyst was reused in five cycles without any significant loss of activity.

© 2013 Elsevier B.V. All rights reserved.

1. Introduction

During the last two decades, with the development of nanotechnology, numerous nanomaterials have been designed and created. Among them, hybrid organic–inorganic materials based on $\text{Fe}_3\text{O}_4@\text{SiO}_2$ core–shell magnetic nanoparticles as special immobilizing carrier of the catalysts' active sites have shown significant contribution to the current researches [1,2]. This is due to their inherent properties such as biocompatibility, easy renewability and recovery by magnetic separation, thermal stability against degradation, large surface area and higher loading of active sites. The aforementioned advantages of $\text{Fe}_3\text{O}_4@\text{SiO}_2$ core–shell magnetic nanoparticles over the other heterogeneous catalysts have brought new opportunities for the design and synthesis of novel solid catalysts [1–3]. Although many investigations have been conducted on the synthesis and characterization of acidic magnetic nanoparticles [4–8], no attention has been paid to combining

hydrophobicity with acidity of materials for providing bifunctional $\text{Fe}_3\text{O}_4@\text{SiO}_2$ core–shell magnetic nanoparticles bearing both sulfonic acid and terminal organic groups protruding on the silica surface of nanocomposites. Introduction of sulfonic acid and organic groups onto the surface of $\text{Fe}_3\text{O}_4@\text{SiO}_2$ core–shell magnetic nanoparticles is interesting since the combination of both functionalities (acidic and hydrophobic) [9–13] allows creation of a less polar organic environment with a relatively strong acidity for acid-catalyzed reactions. In many acid-catalyzed reactions by siliceous based solid acids, the water produced as a by-product is co-adsorbed on the silanol surface of the catalyst [14–22]; thus, the co-adsorbed water poisons the surface of the catalyst and produces more hydrophilic environment, reducing the performance of the catalyst in organic transformations (Scheme 1).

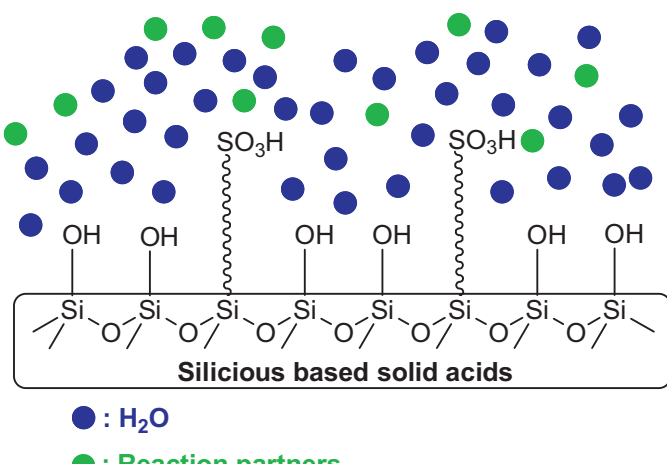
In addition to poisoning of the catalyst's surface in the presence of water molecules as the reaction by-product, the active acidic sites of the catalysts are also subjected to deactivation which inhibits the progress of reactions (Scheme 1) [14–22]. On the other hand, the polarities of the reactants and products, hydrophobic–hydrophilic balance on catalyst's surface, and the acidity of catalysts also have a considerable effect on the reactions' progress. Further research studies addressed the design, synthesis and utilization of the catalytic applications of other surface modified $-\text{SO}_3\text{H}$ solid materials in order to optimize the performance of catalysts [19–26]. As far

* Corresponding author. Tel.: +98 21 23064323; fax: +98 21 22853650.

E-mail addresses: movassagh@kntu.ac.ir (B. Movassagh), [\(B. Karimi\)](mailto:karimi@iasbs.ac.ir).

¹ Tel.: +98 21 23064323; fax: +98 21 22853650.

² Tel.: +98 241 4153225; fax: +98 241 4153232.



Scheme 1. Schematic representation of interaction between water and silanol surface and sulfonic acid active sites of solid acids in water-generating reactions.

as we know, there is not any report about surface hydrophobicity on sulfonic acid-functionalized $\text{Fe}_3\text{O}_4@\text{SiO}_2$ core–shell magnetic nanoparticles; hence, this preliminary work represents the first and a unique example including a hydrophobic $\text{Fe}_3\text{O}_4@\text{SiO}_2@\text{SO}_3\text{H}$ type magnetic material for catalysis in water-generating reactions; thus, offered a new approach to be researched and explored.

As part of our efforts in exploring novel heterogeneous catalysts for organic reactions [23–27], we have designed, prepared and characterized two novel water-tolerant and sulfonic acid organic–inorganic hybrid catalysts based on $\text{Fe}_3\text{O}_4@\text{SiO}_2$ core–shell magnetic nanoparticles: $\text{Fe}_3\text{O}_4@\text{SiO}_2@\text{Et-PhSO}_3\text{H}$ (**1**, Scheme 2) and $\text{Fe}_3\text{O}_4@\text{SiO}_2@\text{Me&Et-PhSO}_3\text{H}$ (**2**, Scheme 2); also, the acidity, hydrophobicity, water-toleration and utility of these catalysts were investigated. In this context, we wish to show that in water-generating reactions involving both hydrophobic and hydrophilic reaction partners, catalyst **2** with hydrophobic character on the surface is much more active and much more robust than catalyst **1**.

2. Experimental

2.1. Chemicals and characterizations

All chemicals were purchased from Merck and Aldrich Chemical Companies. Melting points were determined on a Büchi melting point B-540 apparatus. NMR spectra were recorded at 400 (^1H) and 100.6 (^{13}C) MHz, respectively, on a commercial Bruker DMX-400 instrument using $\text{DMSO}-d_6$ as solvent. IR spectra were recorded on an ABB Bomem Model FTLA 2000 spectrophotometer using KBr discs. The magnetic measurement of samples was carried out in a vibrating sample magnetometer (VSM) (4 in., Daghighe Meghnatis Kashan Co., Kashan, Iran) at room temperature. X-ray diffraction (XRD) patterns were recorded by an Xpert MPD, X-ray diffractometer using $\text{Cu K}\alpha$ radiation. Thermogravimetric and differential thermal analysis (TG-DTA) was carried out using a thermal gravimetric analysis instrument (NETZSCH TG 209F1 Iris) with a heating rate of $10^\circ\text{C min}^{-1}$. SEM was carried out on a VEGA\\TESCAN-LMU instrument. Transmission electron microscope, TEM (Philips CM-10) was also used to obtain TEM images. Elemental analyses for C, H and S were performed using a Heraeus CHN-O Rapid analyzer. The N_2 and H_2O -sorption was carried out in a Belsorp-mini-BEL Japan, Inc. at 298 K (see ESI).

2.2. Preparation of materials

Preparation of $\text{Fe}_3\text{O}_4@\text{SiO}_2$. The synthesis of $\text{Fe}_3\text{O}_4@\text{SiO}_2$ was achieved using the procedure described by Luo and co-workers [28]. This procedure involved a synthetic strategy based on the hydrolysis and condensation of tetraethoxysilane (TEOS) on the surface of Fe_3O_4 magnetic nanoparticles. In a typical preparation procedure, ferric chloride hexahydrate $\text{FeCl}_3 \cdot 6\text{H}_2\text{O}$ (11.0 g, 40.7 mmol) and ferrous chloride tetrahydrate $\text{FeCl}_2 \cdot 4\text{H}_2\text{O}$ (4.0 g, 20.1 mmol) were dissolved in deionized water (250 mL) under nitrogen atmosphere with mechanical stirrer at 85°C . The pH value of the solution was adjusted to 9–11 using aqueous NH_3 (25%). After continuous stirring for 4 h, the magnetite precipitates were washed with distilled water until the pH value descended to 7.0. The black precipitate (Fe_3O_4) was collected with a permanent magnet at the bottom of the reaction flask. The silica coated core–shell magnetic nanoparticles ($\text{Fe}_3\text{O}_4@\text{SiO}_2$ MNPs) were prepared by an ultrasonic pre-mixing of a dispersion of the above black precipitate (2.0 g) with ethanol (400 mL) for approximately 30 min at room temperature. Then, aqueous NH_3 (25%, 12 mL) and TEOS (4.0 mL) were slowly added successively. The resulting solution was mechanically stirred continuously for 24 h, after which the black precipitate product ($\text{Fe}_3\text{O}_4@\text{SiO}_2$) was collected by magnetic separation and washed with ethanol (3 × 15 mL) and dried under vacuum overnight at room temperature (Scheme 2).

Preparation of $\text{Fe}_3\text{O}_4@\text{SiO}_2@\text{Et-PhSO}_3\text{H}$ (1**).** The surface functionalization of the silica coated magnetic nanoparticles with sulfonyl groups was carried out by adding 2-(4-chlorosulfonylphenyl)ethyltrimethoxysilane (CSPETS, 0.4 g, 1.23 mmol) to dry toluene (35 mL) containing silica-coated magnetic nanoparticles (1.0 g). The resulting mixture was stirred for 24 h and then washed with toluene (2 × 15 mL) and distilled water. Finally, the solid was suspended in H_2SO_4 (1 M) solution for 2 h, washed several times with water and dried at room temperature under vacuum overnight to give the corresponding catalyst **1** (Scheme 2).

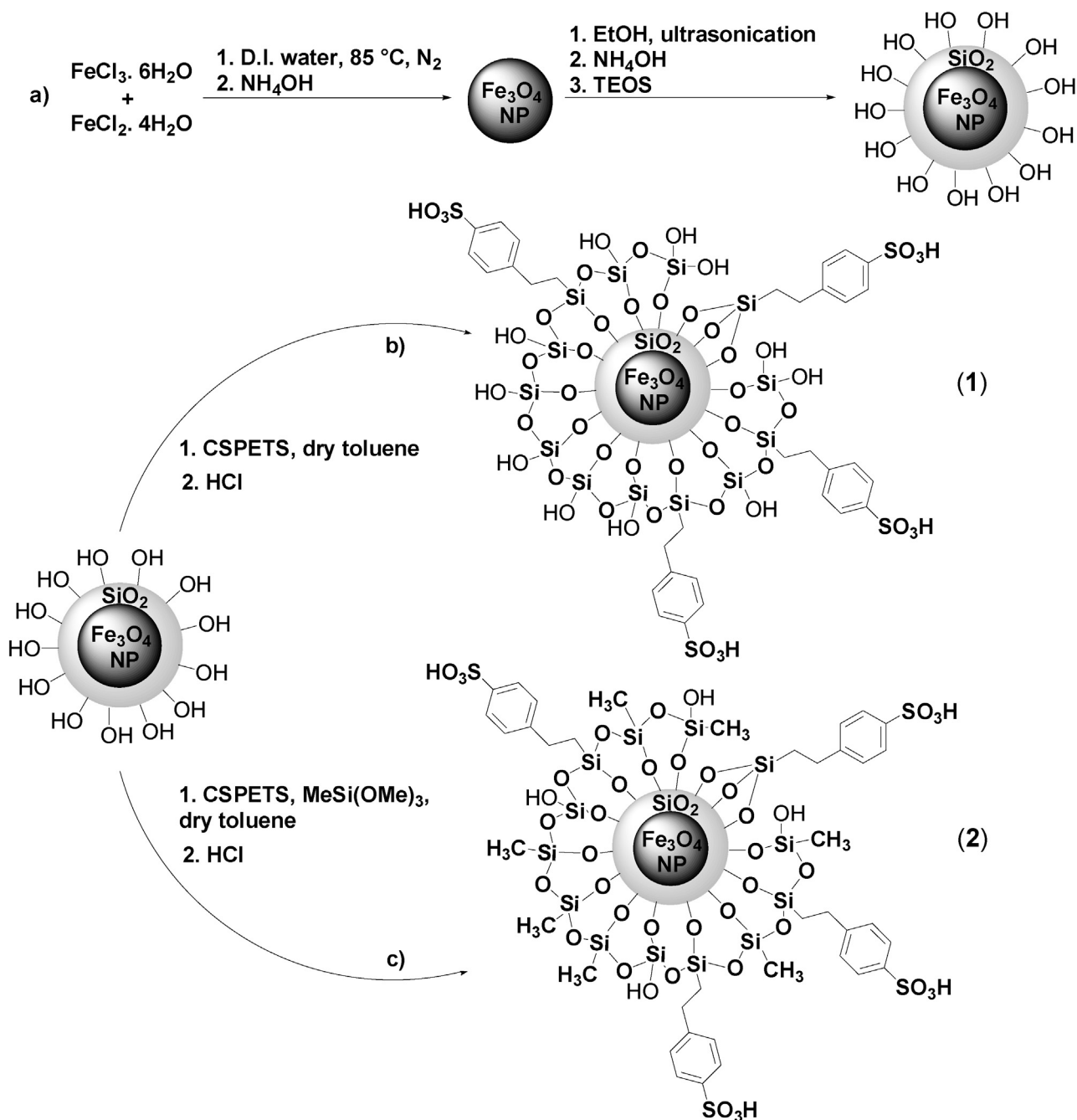
Preparation of $\text{Fe}_3\text{O}_4@\text{SiO}_2@\text{Me&Et-PhSO}_3\text{H}$ (2**).** This procedure involved a synthetic strategy based on the co-condensation of CSPETS and trimethoxymethylsilane (TMMS) on the silica coated magnetic nanoparticles. In a typical preparation procedure, CSPETS (0.2 g, 0.62 mmol) and TMMS (0.2 g, 1.47 mmol) were added to dry toluene (35 mL) containing silica-coated magnetic nanoparticles (1.0 g). The resulting mixture was stirred for 24 h and then washed with toluene (2 × 15 mL) and distilled water. Finally, the solid was suspended in H_2SO_4 (1 M) solution for 2 h, washed several times with water and dried at room temperature under vacuum overnight to give the corresponding catalyst **2** (Scheme 2).

2.3. Acidity of the catalysts (**1** and **2**)

The concentration of sulfonic acid groups was quantitatively estimated by ion-exchange pH analysis [8,28,29]. The catalyst (50 mg) was added to an aqueous solution of NaCl (1 M, 25 mL), and the resulting mixture was stirred for 3 days, after which titration by NaOH (0.05 M) was carried out on the above obtained solutions. The acid amount of **1** and **2** was determined to be 2.22 and 0.70 mmol g^{-1} , respectively.

2.4. General procedure for the one-pot preparation of 3,4-dihydropyrimidin-2-ones/thiones

A mixture of aldehyde (2 mmol), methyl acetoacetate (2 mmol), urea/thiourea (2.4 mmol) and catalyst **2** (7.1 mg, 0.5 mol %) (in the case of thiourea, 1 mol % of the catalyst was used) was stirred at 100°C for an appropriate time under solvent-free condition (Table 3). The progress of the reaction was monitored by thin layer



Scheme 2. Synthetic schemes of (a) Fe_3O_4 NPs and $\text{Fe}_3\text{O}_4 @ \text{SiO}_2$, (b) $\text{Fe}_3\text{O}_4 @ \text{SiO}_2 @ \text{Et-PhSO}_3\text{H}$ (**1**) and (c) $\text{Fe}_3\text{O}_4 @ \text{SiO}_2 @ \text{Me&Et-PhSO}_3\text{H}$ (**2**) core–shell magnetic nanoparticles.

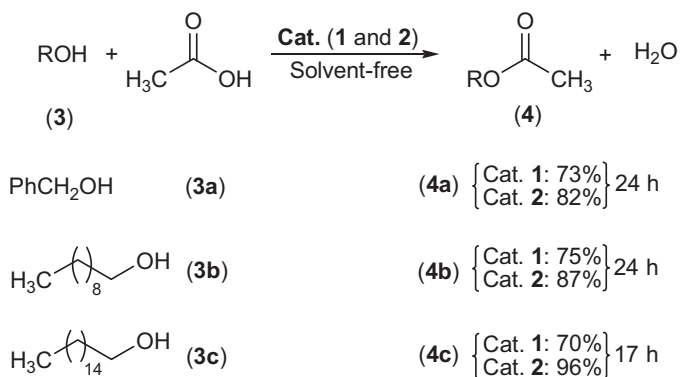
chromatography (TLC). After completion of the reaction, the mixture was washed with water ($3 \times 10 \text{ mL}$). Finally, the mixture was dissolved in hot EtOH and the catalyst was separated by magnetic decantation. The crude product was either recrystallized from EtOH or subjected to preparative thin layer chromatography (silica gel) for further purification.

3. Results and discussion

To examine the effect of surface methyl groups on the catalytic performance of sulfonic acid functionality, catalysts **1** and **2** were tested in the esterification reactions of acetic acid with three alcohols, differing in hydrophobicity. The reaction mixture consisting of acetic acid (3 mmol), alcohol (1 mmol), and catalyst (2 mol%) was heated at 70°C under solvent-free condition. As shown in Scheme 3,

the catalyst **2** exhibited better reactivity compared to the catalyst **1**; moreover, the best result was obtained from the esterification reaction of cetyl alcohol (**3c**) with acetic acid in which the isolated yields of the product (**4c**) were 96% and 70% in the presence of catalysts **2** and **1**, respectively. The enhancement of catalytic properties observed in bifunctional catalyst **2** is attributed to its hydrophobic character, resulting better mass transfer of the reaction partners.

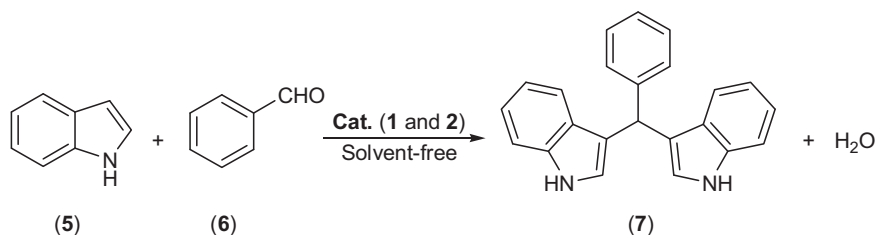
Next, to further probe into the water-tolerance of these solid acids (**1** and **2**) and their catalytic activities, the reaction of indole (**5**) (2 mmol) with benzaldehyde (**6**) (1 mmol) was investigated at 90°C in the presence of these catalysts (1 mol%) under solvent-free condition (Scheme 4). To our delight, we found that after 75 min, catalyst **2** afforded **7** in 94% isolated yield while catalyst **1** gave the same product in 78% yield. This result clearly shown that catalyst **2** is more active than **1**.



Scheme 3. Hydrophobicity assessment of catalysts **1** and **2** in esterification reaction.

In agreement with our hypothesis, the results indicate that the hydrophobic environment on the surface of catalyst **2** not only improved its resistivity against water molecules but also provided easier mass transfer of the reaction partners; hence, they should first diffuse and adsorb on the catalyst's surface and then react at the available active sites. Finally, desorption of the product and extrusion of water molecules from the surface of the catalyst results in a progressive upheaval of the reaction conversion (Fig. 1).

To assess whether the aforementioned results could be generalized to other water-generating reactions, the three-component Biginelli reaction including hydrophobic and hydrophilic substrates, which produce two equivalents of water molecule was also investigated. The Biginelli reaction involves condensation of β -dicarbonyl compounds with aldehydes and urea or thiourea under strongly acidic conditions which is ranked as one of the most recognized and widely employed multi-component reactions (MCRs) for the preparation of 3,4-dihydropyrimidin-2-ones/thiones (DHPMs) [30–37]. DHPMs exhibit a wide variety of biological [38–41] and pharmacological activities such as anticancer, antibacterial,



Scheme 4. Water-tolerance assessment of **1** and **2** in the synthesis of bis(indolyl)methane.

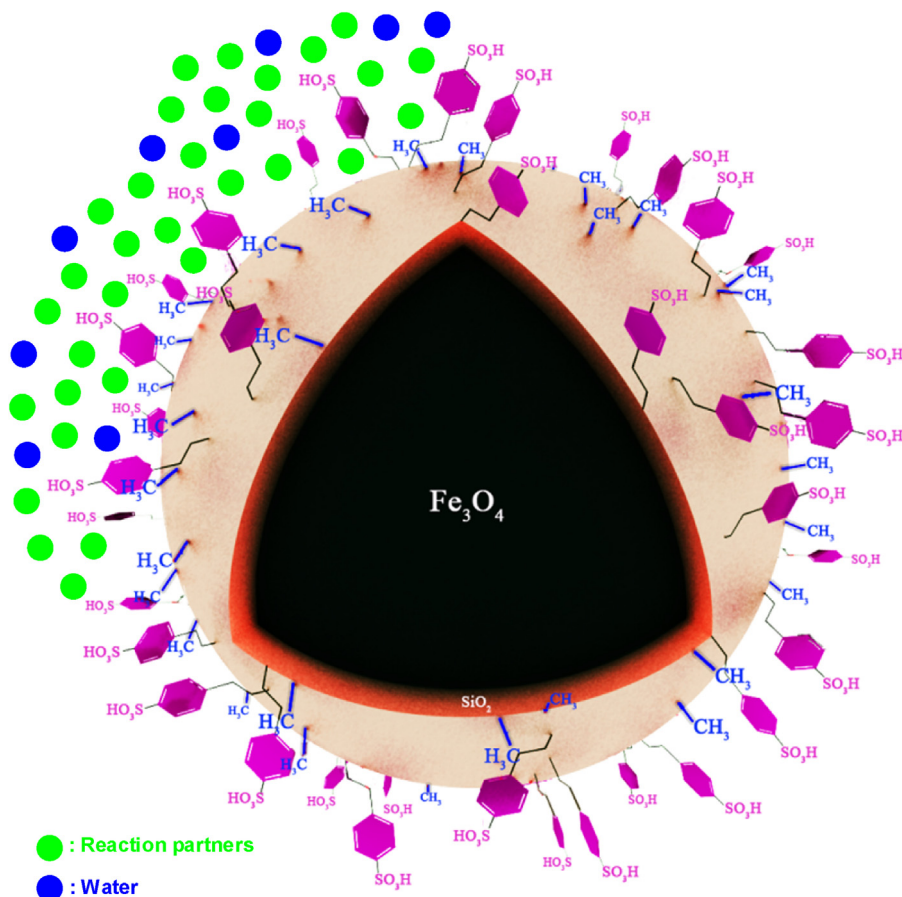


Fig. 1. Schematic demonstration of the mass transfer and water-toleration on the surface of catalyst 2.

antihypertensive, antiviral, potent HIV (gp-120-CD4) inhibitors and calcium channel modulators [42–46].

To test the catalytic capabilities of catalysts **1** and **2**, the Biginelli reaction of methyl acetoacetate (**8**) (2.0 mmol), benzaldehyde (**6**) (2.0 mmol), and urea (**9**) (2.4 mmol) was studied in the presence of the above catalysts (0.5 mol%) at 100 °C. Once again, the catalyst **2** appeared to be much more active than catalyst **1**, affording 90% yield of the desired DHPM (**10a**) in 120 min, while the catalyst **1** gave 83% yield of the same product in 160 min (Scheme 5).

These results clearly show that in addition to previous achievements in esterification and synthesis of bis(indolyl)methane, the catalyst **2** has a superior hydrophobic–hydrophilic and acidity balance in the water-generating reactions; moreover, this catalyst (**2**) with a moderate density of $-\text{SO}_3\text{H}$ sites is an interesting water-tolerant acid catalyst with higher activity by which these reactions can be performed (Fig. 2).

The greater reactivity of catalyst **2** with respect to catalyst **1** is also probably due to a synergistic effect between sufficient hydrophobicity and acidity of siliceous network, which in turn results in the following items:

- (i) Remarkable shielding effect against polar molecules, accessibility of the active sites and easier diffusion of reaction partners within the network resulting from the presence of organic methyl groups on the surface of catalyst **2**.
- (ii) Mild acidic conditions opting for the preparation of DHPMs.

Table 1
Effects of solvent on the catalytic activity of catalyst **2** on the Biginelli reaction with urea.^a

Entry	Solvent	Yield of 10a (%) ^b
1	H_2O	N.R.
2	MeOH	38
3	EtOH	49
4	CH_3CN	64
5	THF	73
6	Toluene	56
7	Dioxane	50

^a Reaction conditions: catalyst **2** (0.5 mol%), benzaldehyde (2 mmol), methyl acetoacetate (2 mmol), urea (2.4 mmol) for 2 h at reflux condition.

^b Yields refer to the isolated pure products.

Similar to the above water-generating reactions, we postulated that the formation of water as a by-product in the Biginelli reaction with either urea or thiourea had inhibited the reaction. As a result, the Biginelli reaction is not efficiently performed by the catalyst **1** because of the hydrophilicity of the surface and high acidity of the catalyst, which in turn, would lead to an enriched water concentration near the active sites during the reaction.

Also, we evaluated the catalytic activity of the catalyst **2** under polar/nonpolar and protic/aprotic conditions (substrates, solvents) to clearly show the bifunctional property and hydrophobicity of the catalyst. In this respect, the performance of the catalyst **2** was investigated in the Biginelli reaction (Table 1). In H_2O , the catalyst **2** was

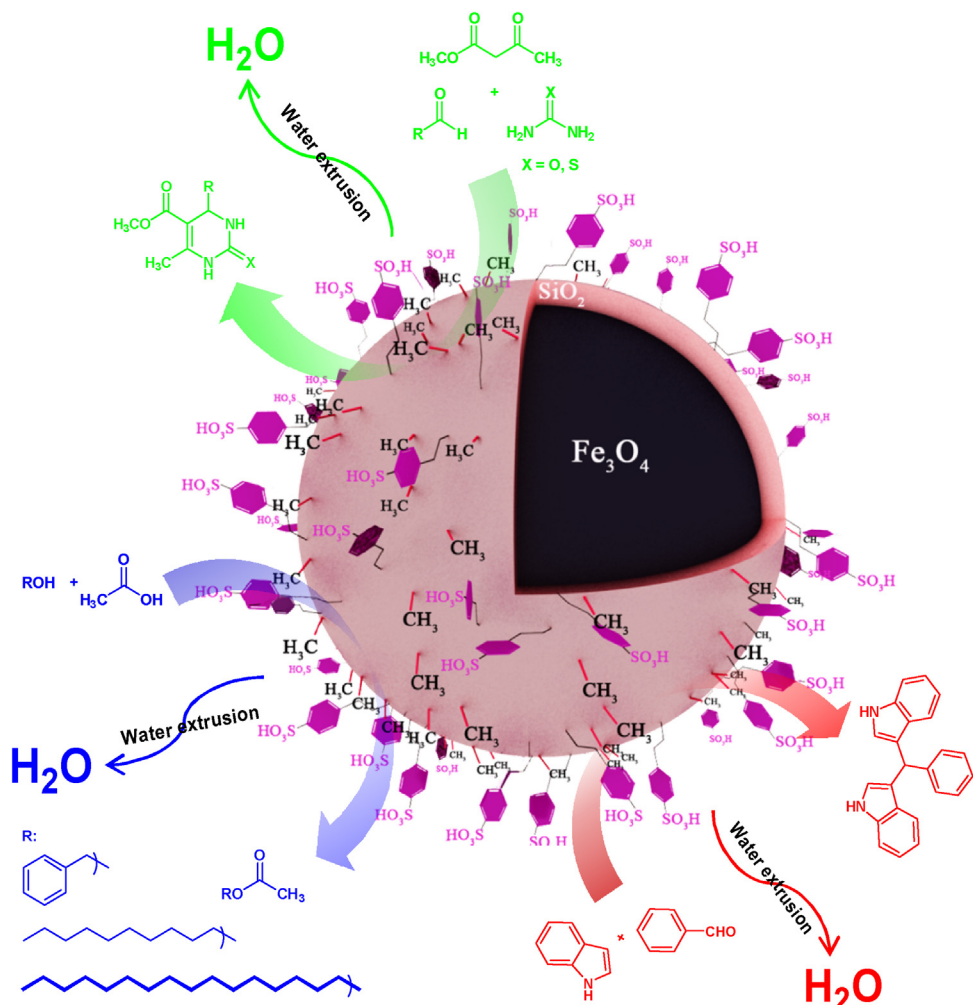
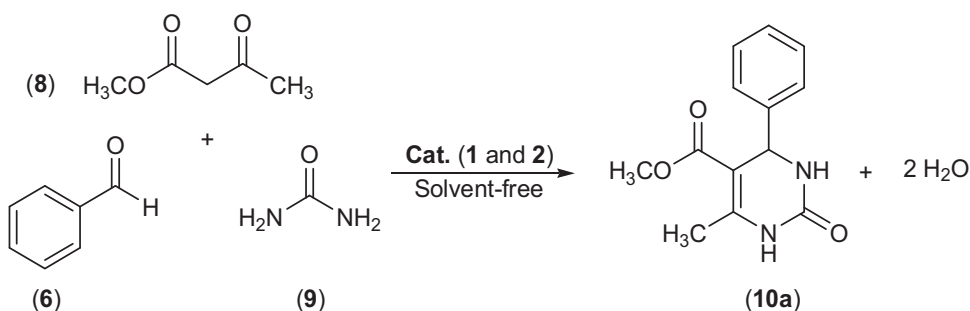


Fig. 2. Water-generating reactions in the presence of the catalyst **2**.



Scheme 5. Water-tolerance and mass transfer assessment of the catalysts (**1** and **2**) in the Biginelli reaction.

not dispersed in the reaction medium and did not participate in the reaction at all (Table 1, entry 1). In other protic solvents, MeOH and EtOH, the progress of the reaction was better, giving the Biginelli adduct in 38% and 49% yields, respectively (Table 1, entries 2 and 3); these results show that protic solvents deactivate the sulfonic acid sites. In acetonitrile, with an aprotic character as well as a dielectric constant higher than the above alcohols, a higher catalytic activity was observed (64%, Table 1, entry 4). In THF, with medium dielectric constant, we saw a better conversion than that of acetonitrile (73%, Table 1, entry 5). Although we saw very good dispersion of the catalyst in toluene (56% isolated yield) and dioxane (50% isolated yield) with low dielectric constants, the solvents were unable to dissolve the polar reactant, urea (Table 1, entries 6–7). These results show that the surface hydrophobicity of the catalyst and the easier diffusion of the reaction partners are better highlighted in the solvent with medium dielectric constant and aprotic character.

To confirm this hypothesis, superior stability and activity of the catalyst **2** over the catalyst **1**, water adsorption–desorption isotherms of catalysts **1** and **2** in the gas phase were measured (Fig. 3). As can be seen in Fig. 2, the surface of catalyst **1** is more hydrophilic than catalyst **2**. Therefore, it is readily poisoned with water molecules, which shows **1** is not a suitable catalyst for the reactions accompanied with water as a by-product. The surface area and surface sorption of catalysts, **1** and **2** were determined by water adsorption–desorption analysis which are summarized in Table 2. The H₂O-sorption isotherms (Fig. 3) and also N₂-sorption isotherms (See ESI) of the synthesized solids exhibited a type IV isotherm pattern with apparent a type H3 hysteresis loops, which are typical of the mesoporous structure with slit-like pores according to the IUPAC classification.

The respective chemical compositions were determined by elemental analysis (carbon and sulfur content measurement) and TGA (Table 2). The C/S ratio for catalysts **1** and **2** obtained by elemental analysis is 3.03 and 4.53, respectively (Table 2) which is quantitatively indicative of more carbon content and more hydrophobicity of the catalyst **2**.

The corresponding structural parameters such as surface area, and total pore volumes were calculated with the Brunauer–Emmet–Teller (BET) method (Table 2). BET surface area

measurements indicated that, compared to the catalyst **1**, the surface area of the catalyst **2** was significantly decreased from 122.3 m² g⁻¹ to 95.8 m² g⁻¹ which was attributed to the surface modification in the catalyst **1** with TMMS precursor. In other words, the reduction of the surface area verifies that the loading of hydrophobic methyl regulator groups has been successful. Moreover, the BET diagram of the catalyst **1** (Fig. 10, ESI) show, 36.434 cm³ g⁻¹ water adsorption while the catalyst **2** (Fig. 17, ESI) show 28.53 cm³ g⁻¹ water adsorption; these data verified our hypothesis and quantitatively indicated the more hydrophobicity of the catalyst **2**.

TGA and DTA with heating from room temperature to 850 °C under argon flow were conducted to determine the amount of organic composition in the modified core–shell Fe₃O₄@SiO₂ materials (Fig. 4). The TGA and DTA profiles of the catalyst **2** showed

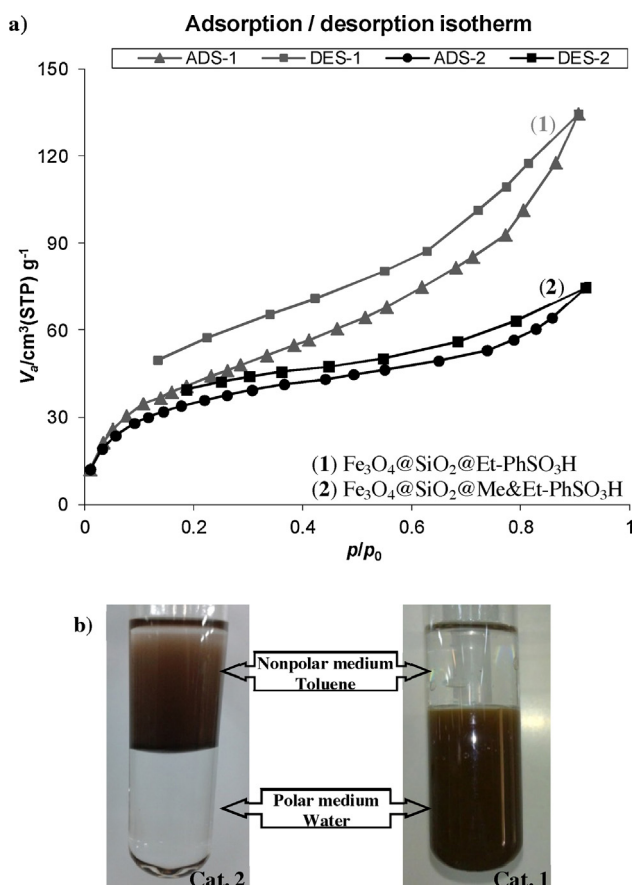


Fig. 3. (a) Water adsorption–desorption isotherms of solid acid catalysts (**1** and **2**). (b) The water tolerance and hydrophobicity of dispersed catalysts (**1** and **2**) in two phase toluene–water systems.

Table 2

Physicochemical and textural properties of sulfonic acid based magnetic nanoparticles.

Entry	Catalyst	$S_{\text{BET}}^{\text{a}}$	V_p^{b}	C (%) ^c	S (%) ^c	C/S	Proton content ^d
1	1	122.36	0.10	6.60	2.18	3.03	2.22
2	2	95.81	0.06	3.17	0.70	4.53	0.72

^a BET surface area (m² g⁻¹).

^b Total pore volume (cm³ g⁻¹).

^c Carbon and sulfur content measured by elemental analysis (w%).

^d Determined by titration after ion-exchange (mmol H⁺ g⁻¹) (see ESI).

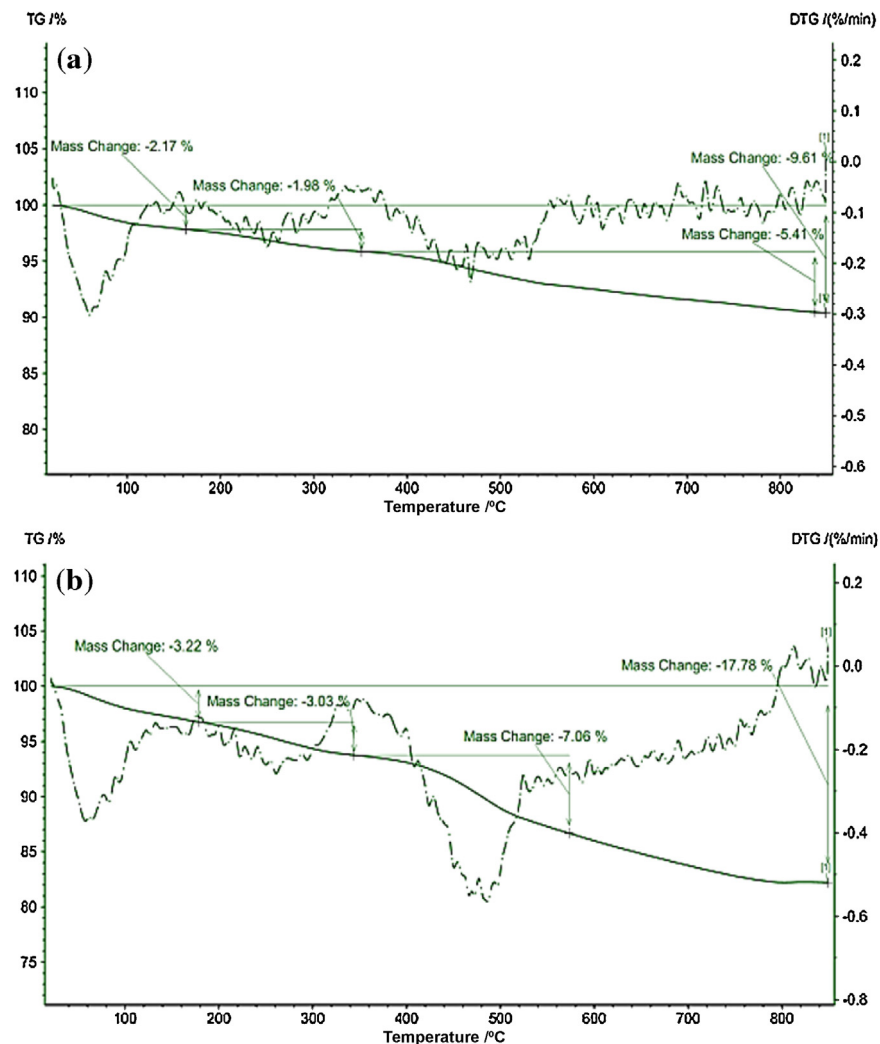


Fig. 4. TGA and DTA diagrams for the catalysts **2** (a), and **1** (b).

weight losses peaks around 0–160, 160–360, and 360–860 °C which were assigned to the desorption of physisorbed water, surface methyl groups and organosulfonic acid decomposition, respectively (Fig. 4a); the TGA and DTA profiles of the catalyst **1** showed weight losses peaks around 0–160, 160–360, 360–580 and 580–860 °C, which were assigned to the desorption of physisorbed water and organosulfonic acid decomposition (Fig. 4b).

The textural properties of the functionalized organic–inorganic hybrid catalysts synthesized for the current work were determined by XRD, VSM, SEM and TEM.

The XRD pattern of the Fe₃O₄ (Fig. 5a), Fe₃O₄@SiO₂ (Fig. 5b), catalysts **1** and **2** (Fig. 5c and d, respectively) exhibited diffraction peaks around 30.09, 35.42, 43.11, 53.72, 57.7, 62.73, 71.23, and 74.22, corresponding to the Miller indices values {*hkl*} of {200}, {311}, {400}, {422}, {511}, {440}, {620}, and {533}, respectively; these values are in good agreement with the standard XRD pattern of Fe₃O₄ (JCPDS file No. 19-0629) indicating the retention of the crystalline structure during functionalization of MNPs. The weak broad band ($2\theta = 18\text{--}27^\circ$) in the Fe₃O₄@SiO₂, catalyst **1**, and catalyst **2** samples could be assigned to the amorphous silica shell formed around the Fe₃O₄ magnetic nanoparticle cores (Fig. 5b–d). However, we do not expect to see marked differences among hybrid organic–inorganic catalysts **1** and **2** (Fig. 5c and d), inorganic matrix Fe₃O₄@SiO₂ (Fig. 5b) and Fe₃O₄ (Fig. 5a); this is because there is not any crystalline structure for the organic pendants on the catalysts'

surfaces. Moreover, Fig. 5c–d shows that the crystalline structures of the core–shell Fe₃O₄@SiO₂ have not been changed despite being modified with organic precursors.

In order to investigate the crystalline nature and morphological features of the catalyst **2**, scanning electron microscopy (SEM) and transmission electron microscopy (TEM) were carried out. SEM image of the catalyst showed that they were floccules without having a regular structure. On the other hand, the surface of these particles was non-smooth, which resulted in an increase in the surface areas of these particles. In these cases, the TEM images provide more accurate information on the particle size and morphology of MNPs, therefore, these images were investigated. TEM observations clearly reveal the core–shell structure of the nanoparticles. Due to different electron density, these images display a dark nano-Fe₃O₄ core about 17 nm in diameter surrounded by a gray silica shell about 7 nm thick, moreover, the average catalyst particle diameter is about 24 nm (Fig. 6).

The magnetic properties of the neat Fe₃O₄ NPs and catalyst **2** were evaluated at room temperature and the VSM magnetization curves of magnetic nanoparticles, before and after functionalization, exhibited a superparamagnetic character of Fe₃O₄ NPs, and core–shell magnetic Fe₃O₄@SiO₂@Me&Et-PhSO₃H catalyst (**2**) (Fig. 7a). The magnetic saturation of the catalyst **2** (36.8 emu/g) was less than that of bare Fe₃O₄ (66.96 emu/g); this reduced magnetic strength is due to the silica shells coated on magnetic particles.

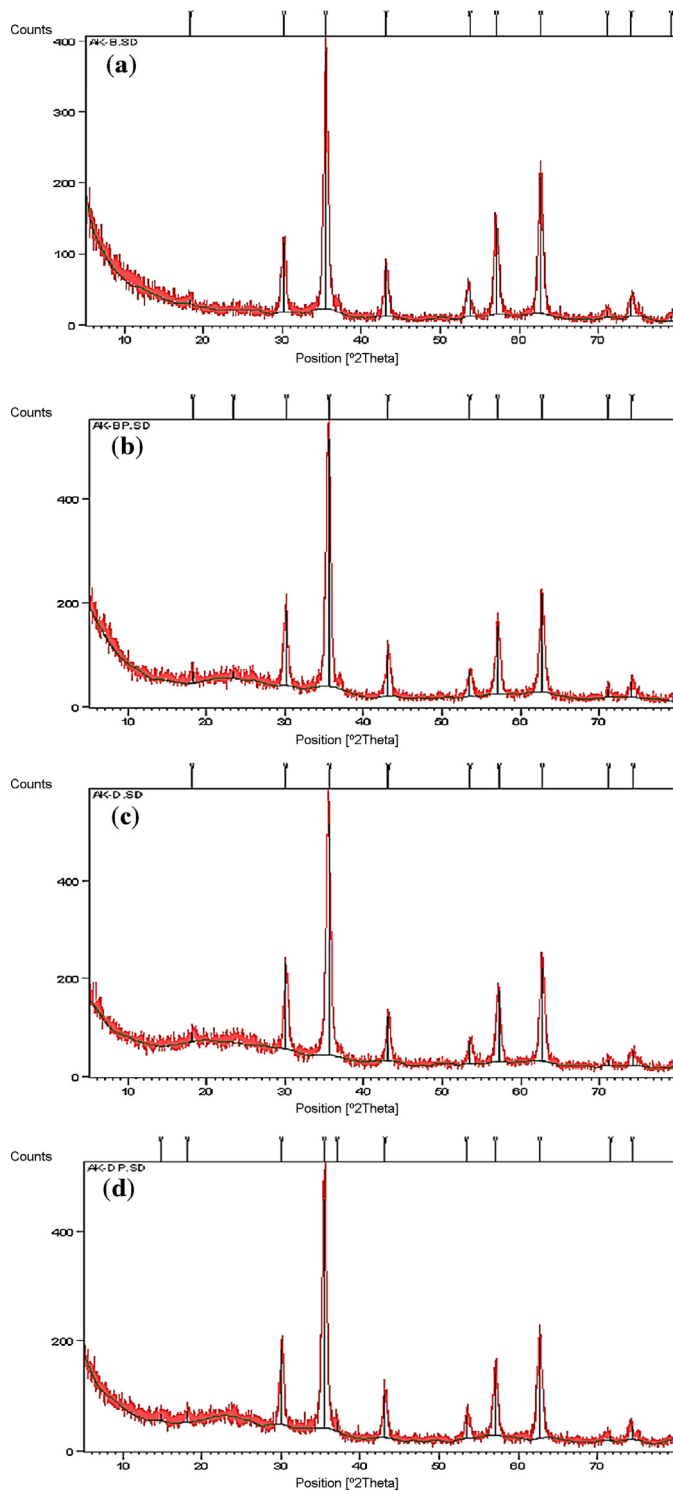


Fig. 5. Powder XRD patterns: (a) Fe_3O_4 ; (b) $\text{Fe}_3\text{O}_4@\text{SiO}_2$; (c) 1 and (d) 2 magnetite nanoparticles.

However, the magnetization value was sufficient for common magnetic separation. The strong magnetization of the nanoparticles was also tested by simple attraction using an external magnet (Fig. 7b).

Also, FT-IR spectroscopy was employed to verify the synthesized blank Fe_3O_4 MNPs, $\text{Fe}_3\text{O}_4@\text{SiO}_2$ core–shell MNPs and the other core–shell surface modified samples (Fig. 8). FT-IR Spectra of the bare magnetic Fe_3O_4 nanoparticles displayed a characteristic absorption peak of $\text{Fe}–\text{O}$ bond at about 590 cm^{-1} (Fig. 8a). The absorption peaks of the silica shell in the $\text{Fe}_3\text{O}_4@\text{SiO}_2$ core–shell

Table 3

Effects of reaction temperature and mol% of the catalyst **2** on the Biginelli reaction with urea.^a

Entry	Catalyst (mol%)	Temperature (°C)	Time (h)	Yield of 10a (%) ^b
1	1	50	8	44
2	1	70	5	85
3	1	90	2	93
4	0.7	90	2.8	92
5	0.5	90	4.75	88
6	0.5	100	2	90
7	0.5	110	1.7	91
8	0.3	110	3.6	89

^a Reaction conditions: benzaldehyde (2 mmol), methyl acetoacetate (2 mmol), urea (2.4 mmol).

^b Yields refer to the isolated pure products.

magnetic nanoparticles around 1092 and 801 cm^{-1} correspond to the antisymmetric and symmetric stretching vibrations of $\text{Si}–\text{O}–\text{Si}$ bond in oxygen–silica tetrahedral, respectively (Fig. 8b). The presence of the anchored alkyl groups is confirmed by the aliphatic weak $\text{C}–\text{H}$ stretching vibrations appearing at 2922 cm^{-1} in the catalyst **2** and 2926 cm^{-1} in the catalyst **1**.

An increase in intensity and broadening of the band at 3000 – 3500 cm^{-1} in the samples suggests that there are more OH groups on the magnetic nanoparticle surface after the modification and sulfonation. Thus the above results indicate that the functional groups were successfully grafted on the surface of the $\text{Fe}_3\text{O}_4@\text{SiO}_2$ nanoparticles.

In order to find the best reaction conditions, we first examined the effect of temperature with constant loading of the catalyst (1 mol%). It was found that the yield of the desired 3,4-dihydropyrimidin-2-one was raised at higher temperature in shorter reaction times (Table 3, entries 1–3). Also, reducing the amount of the catalyst did not have any significant impact on the product yields at $90\text{ }^\circ\text{C}$ (Table 3, entries 4 and 5). We also examined the effect of temperatures $>90\text{ }^\circ\text{C}$ and lower loadings of the catalyst to show high performance of the catalyst **2** in the reaction (Table 3, entries 6–8). It gave the expected product in a good yield. It was concluded that solvent-free conditions at $100\text{ }^\circ\text{C}$ in the presence of 0.5 mol% of the catalyst **2** is the optimized condition for this three-component reaction (Table 3, entry 6).

Since thiopyrimidinones are important pharmacophores with regard to biological activity [35,39], our next objective was to develop an efficient procedure for their synthesis using thiourea as one of the reactants (Scheme 6). The aforementioned optimized conditions were not successful when thiourea (**11**) was used instead of urea; therefore, the reaction was performed with higher concentration of the catalyst (1 mol%), at $100\text{ }^\circ\text{C}$ for 8 h, thus affording 91% isolated yield of **12a**.

With the optimized reaction conditions in hand, the generality of the procedure for the Biginelli adducts was investigated with various aldehydes and urea/thiourea and a library of substituted DHPMs was obtained in high to excellent yields in appropriate reaction times under solvent-free conditions (Table 4).

Both electron-withdrawing as well as electron-donating substituents on the aldehyde aryl ring were tolerated which, in turn, reacted with methyl acetoacetate and urea/thiourea under the optimized conditions. *Meta*- and *para*-fluoro and *meta*-bromobenzaldehydes successfully produced the desired products in similarly excellent yields (Table 4, entries 2–4) indicating that the position of the electron-withdrawing substituent had no significant effect on the yield. A similar behavior was observed with electron-releasing groups, *meta*-methyl (Table 4, entry 5), *para*-isopropyl (Table 4, entry 6), *meta*- and *para*-hydroxy (Table 4, entries 7 and 8) and *para*-methoxy (Table 4, entry 9) benzaldehydes produced the expected DHPMs in high to excellent

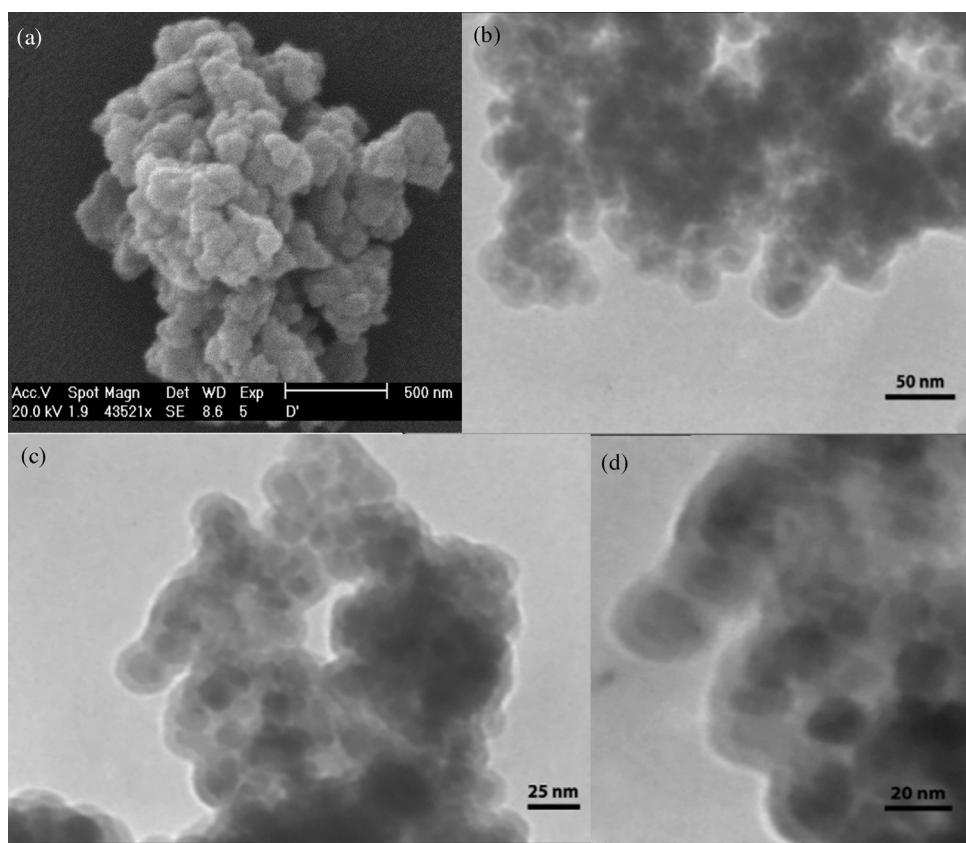
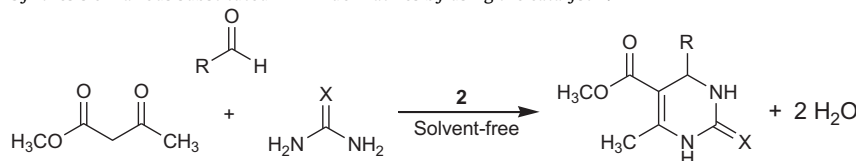


Fig. 6. SEM (a) and TEM (b-d) images of the catalyst **2** magnetic core–shell nanoparticles.

Table 4

Synthesis of various substituted DHPM derivatives by using the catalyst **2**.^a

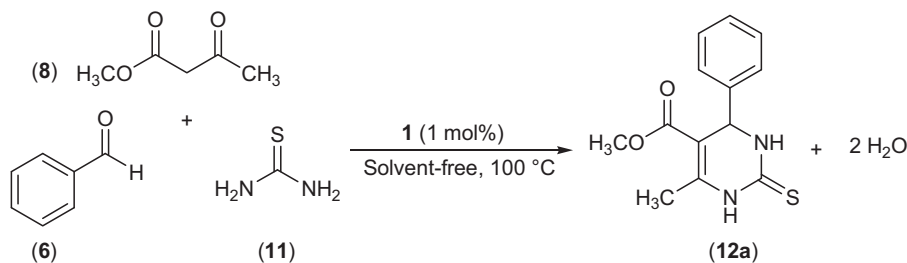
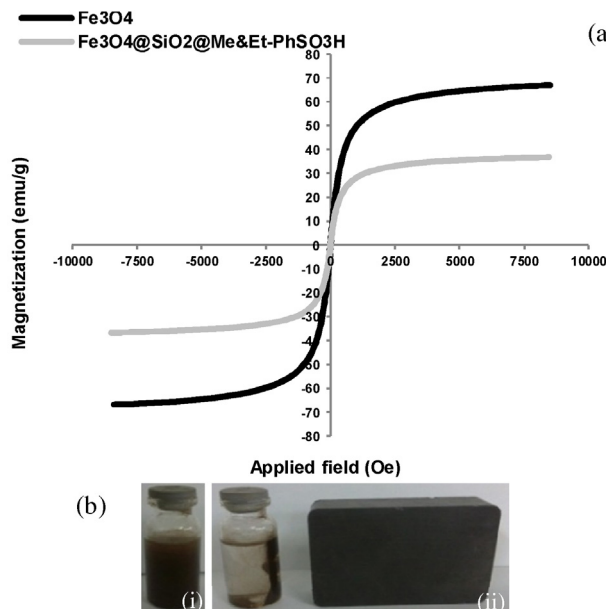


Entry	Aldehyde	X	Time (h)	Yield (%) ^b	Product
1	Benzaldehyde	O	2	90	10a
2	3-Fluorobenzaldehyde	O	1.9	92	10b
3	4-Fluorobenzaldehyde	O	2	90	10c
4	3-Bromobenzaldehyde	O	2.17	91	10d
5	3-Methylbenzaldehyde	O	2.3	93	10e
6	4-Isopropylbenzaldehyde	O	2.5	91	10f
7	3-Hydroxybenzaldehyde	O	2.3	86	10g
8	4-Hydroxybenzaldehyde	O	2.3	88	10h
9	4-Methoxybenzaldehyde	O	2.5	89	10i
10	1-Naphthaldehyde	O	1.8	93	10j
11	Anthracene-10-carbaldehyde	O	2	88	10k
12	3-Phenylpropionaldehyde	O	3.7	89	10l
13	Thiophene-2-carbaldehyde	O	1.9	88	10m
14	Benzaldehyde	S	8	91 ^c	12a
15	3-Fluorobenzaldehyde	S	8	91 ^c	12b
16	4-Fluorobenzaldehyde	S	8.17	92 ^c	12c
17	3-Methylbenzaldehyde	S	8.5	91 ^c	12d
18	3-Bromobenzaldehyde	S	8	89 ^c	12e
19	4-Isopropylbenzaldehyde	S	8.75	90 ^c	12f
20	4-Methoxybenzaldehyde	S	9.25	87 ^c	12g
21	1-Naphthaldehyde	S	7.5	90 ^c	12h
22	3-Phenylpropionaldehyde	S	9.75	82 ^c	12i

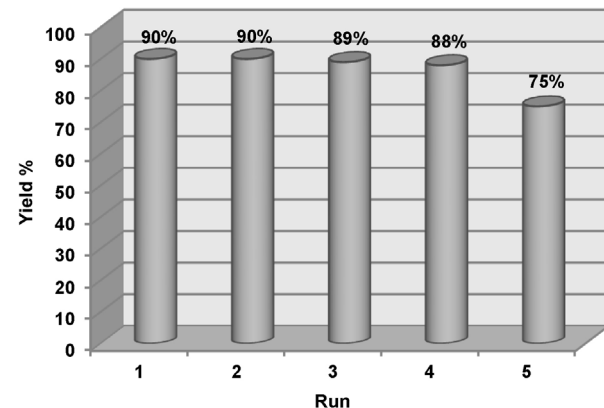
^a Reaction conditions: aldehyde (2 mmol), methyl acetoacetate (2 mmol), urea or thiourea (2.4 mmol) and **2** (0.5 mol%) at 100 °C.

^b Yields refer to the isolated pure products based on aldehydes.

^c Reaction was carried out using 1 mol% of **2**.

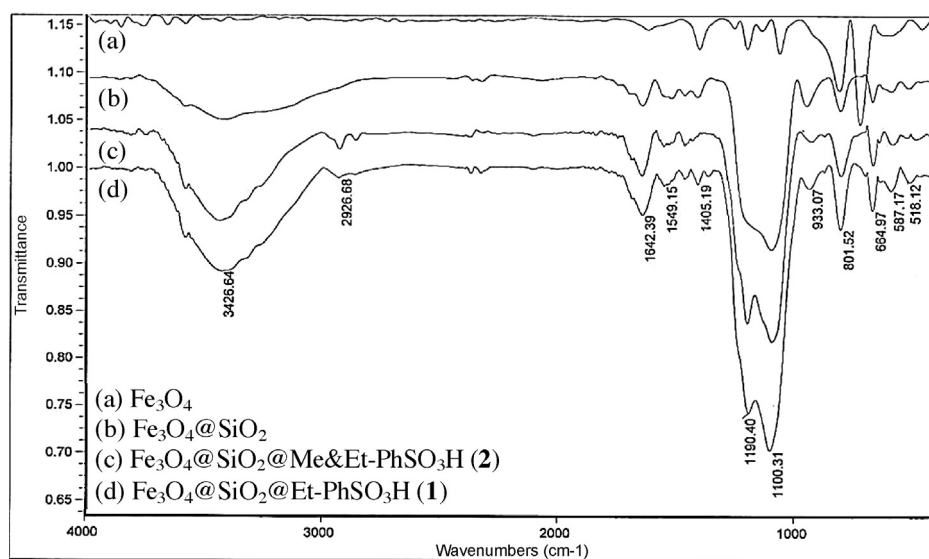
**Scheme 6.** Biginelli reaction with thiourea.**Fig. 7.** (a) Magnetization (M) as a function of field (H) for Fe_3O_4 nanoparticles (black curve) and **2** (gray curve). (b) The catalyst **2** in a typical reaction mixture in the absence (i) and the presence of a magnetic field.

yields. Also, bulky aromatic 1-naphthaldehyde and anthracene-10-carbaldehyde showed remarkable performances (Table 4, entries 10 and 11). Furthermore, under similar reaction conditions, 3-phenylpropionaldehyde, a model for aliphatic and enolizable

**Fig. 9.** Recyclability of the catalyst **2** for the Biginelli reaction of benzaldehyde, methyl acetoacetate and urea.

aldehyde, gave the corresponding DHPM in high yield (Table 4, entry 12). It is noteworthy that the methodology was also successful for heterocyclic thiophene-2-carbaldehyde (Table 4, entry 13). Then, we replaced urea with thiourea and were pleased to find that this three-component reaction was also catalyzed by **2** in excellent yields (Table 4, entries 14–22).

The recovery of the catalyst **2** (0.5 mol%) in the Biginelli reaction of benzaldehyde (2 mmol) with methyl acetoacetate (2 mmol) and urea (2.4 mmol) under solvent-free condition for 2 h at 100 °C was tested. Upon completion of the reaction, the mixture was washed with water (30 mL). After decantation of washing water the solid mixture was dissolved in hot EtOH and the catalyst was easily

**Fig. 8.** FT-IR spectra for the Fe_3O_4 nanoparticles (a), $\text{Fe}_3\text{O}_4@\text{SiO}_2$ (b), catalyst **2** (c), and catalyst **1** (d).

separated and recovered from the reaction mixture by an external magnet, washed with water and ethanol and finally dried at 110 °C for 1 h prior to the next run. During the recycling experiment with fresh reactants, under the same reaction conditions, no considerable change in the activity of the catalyst was observed for at least 5 consecutive runs which clearly demonstrate the stability of the catalyst for these conditions in the Biginelli reaction (Fig. 9). It is very important to note that for the reactions in which water participates as a by-product, only a few solid acids show acceptable performance and stability [22].

4. Conclusions

In summary, we have designed, prepared and characterized two novel organosulfonic acid functionalized silica-coated magnetic nanoparticles (**1** and **2**) with dual functionality comprised of both hydrophobicity and acidity properties. The activity of the catalysts was tested in three water-generating transformations namely: acid-catalyzed esterification reaction of fatty alcohols, synthesis of bis(indolyl)methane, and the Biginelli reaction. Moreover, the performance of the catalysts was investigated with regards to hydrophobicity and water-toleration of the catalysts' surface and also mass transfer of the reaction partners. It has been shown that the catalyst **2** containing methyl groups on the surface is much more active than the catalyst **1**. Shielding effects of the methyl groups bounded to the surface of the catalyst **2** having sulfonic acid sites prompted water-tolerance of the catalyst and water extrusion from the surface, resulting in prevention of deactivation of sulfonic active sites by water as the reaction by-product. Finally, the catalytic activity and the ability to recycle and reuse were studied on the catalyst **2**. Comparative outcomes on the performances of the catalysts (**1** and **2**) expand the capability of the catalysts and anticipate further progress by creative research to explore the surface hydrophobicity of magnetic catalysts.

Acknowledgments

This work was supported by the Research Council of the K. N. Toosi University of Technology. The authors express their gratitude to Dr. Sogand Noroozizadeh for editing the English content of this manuscript.

References

- [1] V. Polshettiwar, R. Luque, A. Fihri, H. Zhu, M. Bouhrara, J.M. Basset, Chem. Rev. 111 (2011) 3036–3075.

- [2] S. Shylesh, V. Schnemann, W.R. Thiel, Angew. Chem. Int. Ed. 49 (2010) 3428–3459.
- [3] A.H. Lu, E.L. Salabas, F. Schuth, Angew. Chem. Int. Ed. 46 (2007) 1222–1244.
- [4] A. Pourjavadi, S.H. Hosseini, M. Doulabi, S.M. Fakoorpoor, F. Seidi, ACS Catal. 2 (2012) 1259–1266.
- [5] Y.H. Liu, J. Deng, J.W. Gao, Z.H. Zhang, Adv. Synth. Catal. 354 (2012) 441–447.
- [6] Q. Zhang, H. Su, J. Luo, Y. Wei, Green Chem. 14 (2012) 201–208.
- [7] N. Koukabi, E. Kolvari, M.A. Zolfigol, A. Khazaei, B.S. Shaghaseemi, B. Fasahati, Adv. Synth. Catal. 354 (2012) 2001–2008.
- [8] M.Z. Kassaee, H. Masrouri, F. Movahedi, Appl. Catal. A: Gen. 359 (2011) 28–33.
- [9] F. Liu, W. Kong, C. Qi, L. Zhu, F.S. Xiao, ACS Catal. 2 (2012) 565–572.
- [10] F. Liu, L. Wang, Q. Sun, L. Zhu, X. Meng, F.S. Xiao, J. Am. Chem. Soc. 134 (2012) 16948–16950.
- [11] W. Long, C.W. Jones, ACS Catal. 1 (2011) 674–681.
- [12] C.H. Tsai, H.T. Chen, S.M. Althaus, K. Mao, T. Kobayashi, M. Pruski, V.S.Y. Lin, ACS Catal. 1 (2011) 729–732.
- [13] Q. Yang, M.P. Kapoor, S. Inagaki, J. Am. Chem. Soc. 124 (2002) 9694–9695.
- [14] J. Mondal, T. Sen, A. Bhaumik, Dalton Trans. 41 (2012) 6173–6181.
- [15] F.J. Liu, X.J. Meng, Y.L. Zhang, L.M. Ren, F. Nawaz, F.-S. Xiao, J. Catal. 271 (2010) 52–58.
- [16] J. Liu, J. Yang, C.M. Li, Q. Yang, J. Porous Mater. 16 (2009) 273–281.
- [17] J.A. Melero, L.F. Bautista, G. Morales, J. Iglesias, D. Briones, Energy Fuels 23 (2009) 539–547.
- [18] G. Morales, G. Athens, B.F. Chmelka, R. van Grieken, J.A. Melero, J. Catal. 254 (2008) 205–217.
- [19] I.K. Mbaraka, B.H. Shanks, J. Catal. 229 (2005) 365–373.
- [20] Q. Yang, J. Liu, M.P. Kapoor, S. Inagaki, C. Li, J. Catal. 228 (2004) 265–268.
- [21] I.K. Mbaraka, D.R. Radu, V.S.Y. Lin, B.H. Shanks, J. Catal. 219 (2003) 329–336.
- [22] T. Okuhara, Chem. Rev. 102 (2002) 3641–3666.
- [23] M. Navidi, B. Movassagh, S. Rayati, Appl. Catal. A: Gen. 452 (2013) 24–28.
- [24] B. Karimi, H.M. Mirzaei, A. Mobaraki, Catal. Sci. Technol. 2 (2012) 828–834.
- [25] B. Karimi, M. Vafeezadeh, Chem. Commun. 48 (2012) 3327–3329.
- [26] B. Karimi, D. Zareyee, J. Mater. Chem. 19 (2009) 8665–8670.
- [27] B. Karimi, D. Zareyee, Org. Lett. 10 (2008) 3989–3992.
- [28] Q. Zhang, H. Su, J. Luo, Y. Wei, Green Chem. 14 (2012) 201–208.
- [29] E.G. Derouane, J.C. Védrine, R.R. Pinto, P.M. Borges, L. Costa, M.A.N.D.A. Lemos, F. Lemos, F.R. Ribeiro, Catal. Rev.: Sci. Eng. 55 (2013) 454–515.
- [30] P. Biginelli, Gazz. Chim. Ital. 23 (1893) 360–416.
- [31] H.G.O. Alvim, T.B. De-Lima, H.C.B. De-Oliveira, F.C. Gozzo, J.L. De-Macedo, P.V. Abdelnur, W.A. Silva, B.A.D. Neto, ACS Catal. 3 (2013) 1420–1430.
- [32] S. Gore, S. Baskaran, B. Koenig, Green Chem. 13 (2011) 1009–1013.
- [33] G.C. Tron, A. Minassi, G. Appendino, Eur. J. Org. Chem. (2011) 5541–5550.
- [34] H. Murata, H. Ishitani, M. Iwamoto, Org. Biomol. Chem. 8 (2010) 1202–1211.
- [35] J.P. Wan, Y.J. Pan, Chem. Commun. (2009) 2768–2770.
- [36] Z.J. Quan, Y.X. Da, Z. Zhang, X.C. Wang, Catal. Commun. 10 (2009) 1146–1148.
- [37] R. Gupta, S. Paul, R. Gupta, J. Mol. Catal. A: Chem. 266 (2007) 50–54.
- [38] H.Y.K. Kaan, V. Ulaganathan, O. Rath, H. Prokopcova, D. Dallinger, C.O. Kappe, F. Kozielski, J. Med. Chem. 53 (2010) 5676–5683.
- [39] M.A. Blasco, S. Thumann, J. Wittmann, A. Giannis, H. Groger, Bioorg. Med. Chem. Lett. 20 (2010) 4679–4682.
- [40] R.F.S. Canto, A. Bernardi, A.M.O. Battastini, D. Russowsky, V.L. Eifler-Lima, J. Braz. Chem. Soc. 22 (2011) 1379–1388.
- [41] H.L. Luo, W. Yang, Y. Li, S.F. Yin, Chem. Nat. Compd. 46 (2010) 412–416.
- [42] I. Garcia-Saez, S. De-Bonis, R. Lopez, F. Trucco, B. Rousseau, P. Thuery, F. Kozielski, J. Biol. Chem. 282 (2007) 9740–9747.
- [43] B. Jauk, T. Pernat, C.O. Kappe, Molecules 5 (2000) 227–239.
- [44] C.O. Kappe, Eur. J. Med. Chem. 35 (2000) 1043–1052.
- [45] C.O. Kappe, Molecules 3 (1998) 1–9.
- [46] L.E. Overman, M.H. Rabinowitz, P.A. Renhowe, J. Am. Chem. Soc. 117 (1995) 2657–2658.